

Optimal Design of $FPI^{\lambda}D^{\mu}$ based Stabilizers in Hybrid Multi-Machine Power System Using GWO Algorithm

A. Nateghi¹, H. Shahsavari^{2,*}

¹ Department of Electrical Engineering, Shahid Sattari Aeronautical University, Tehran, Iran

² Department of Electrical Engineering, Azarbaijan Shahid Madani University, Tabriz, Iran

Abstract- In this paper, the theory and modeling of large scale photovoltaic (PV) in the power grid and its effect on power system stability are studied. In this work, the basic module, small signal modeling and mathematical analysis of the large scale PV jointed multi-machine are demonstrated. The principal portion of the paper is to reduce the low frequency fluctuations by tuned stabilizer in the attendance of the PV unit. In order to optimize the system performance, a novel optimal fuzzy based fractional order PID ($FPI^{\lambda}D^{\mu}$) stabilizers are proposed to meliorate small signal stability of a power network connected PV unit. For optimizing the performance of the system, $FPI^{\lambda}D^{\mu}$ is exploited by Gray Wolf Optimization (GWO) algorithm. In order of evaluation of the proposed stabilizers performance, two different types of controllers are compared, include optimal classic stabilizer and $FPI^{\lambda}D^{\mu}$ based particle swarm optimization (PSO) algorithm. The superiority of $FPI^{\lambda}D^{\mu}$ based GWO on improving small signal stability in the studied system, including large scale PV is shown via time-domain simulations.

Keyword: Fractional order PID ($PI^{\lambda}D^{\mu}$) controller; Fuzzy Control; Photovoltaic; Gray Wolf Optimization (GWO) Algorithm; Small Signal Model.

1. INTRODUCTION

The renewable generations in the providing of energy in distant places and the diminution of fossil usage [1-3] have an essential role in power systems [4]. The main problem is about the alternative essence of the renewable generations, which effect on the power system stability [5]. One of the best types of renewable energies, which produce power by changing radiation to electricity is a Photovoltaic (PV) panels. It is clear that in the next decades, the large scale PV will be considered as source power production in the transmission grid. International energy agency-photovoltaic technology plan (IEA-PVT) introduced the large-size PV power plant from 10 MW up to several GW in a zone from 0.1 to 20 km² [6]. The large-scale penetration of the PV power plant into power grids will remarkably affect power transmission and generation systems [7]. Accordingly, the efficacy of large scale PV on small signal power system stability is very

significant and should be studied carefully [8-10]. Till now, there have been many publications about the PV power unit on the low frequency analysis of the distribution system. The effects of high penetration of the PV unit on distribution grids have been published in Refs. [11-14]. As these researches propose, high influence of PV power can effect on the voltage profile depending on the level of power PV infiltration and the loading conditions. Study outcomes of these researches propose that the voltage regulation equipment which presently available is not able to damp down the harmful effects of PV system transients. With the increase in PV infiltration, the affect of these systems on the transmission networks cannot be ignored, while a few studies have been performed about the efficacy of high capacity PV on the transmission system. Researchers [15-18] have studied the transient conduct of the transmission system in repercussion to different perturbations related to PV unit. In Ref. [15], Authors study the effect of PV influence and STATCOM on the stability of a single machine infinite bus (SMIB) system based on the rotor angle stability. It has been illustrated in Ref. [16] that depending on the level of PV power production, PV power production can have both effective and adverse effects on transient voltages. Ref. [17] presents a cost efficient control algorithm for standalone batteryless PV systems. Authors in Ref. [18]

Received: 18 Aug. 2019

Revised: 12 Nov. 2019

Accepted: 28 Nov. 2019

*Corresponding author:

E-mail: hosinshahsavari@gmail.com (H. Shahsavari)

DOI: 10.22098/joape.2021.6392.1481

Research paper

© 2021 University of Mohaghegh Ardabili. All rights reserved.

investigate the effect of BESS on low frequency oscillations in multi-machine power system with large-size PV penetration. In Ref. [19], in order to see both harmful and beneficial effects of PV power generation on the stability of a power system under increased levels of PV power generation is perused. The stability of the voltage and angle of a PV system connected IEEE 14 bus system is studied in Ref. [20]. The impact of PV plants on low frequency fluctuations is also studied in this work. Authors in Ref. [21] design a SMIB system with the grid-connected large-size PV power plant due to investigate the influence of a grid-connected PV power plant on the small signal stability. They illustrate the effect of the size of the PV injected power production to the network on the damp torque. It causes a negative or positive effect on small frequency oscillations, although not argued about how to control the system. A complementary control signal in the excitation system of a generating unit can be used in order to provide fast damping for this complicated system and improve its dynamic stability. Dynamic analysis of large-size PV plant in the power system and damp out the electromechanical fluctuations by a novel controller, is the main target of this paper. The inertia-less large scale PVs put extra load on the formal synchronous generators in power network which have to inject the determinate damping torque to insure stability of the system. The power system stabilizers (PSSs) provide appropriate consolidation signals over an extensive range of oscillations and operating situations [22]. With the development of the PV and increment uncertainty of power generated in the transmission power network, the abrupt perturbation causes the instable system or feeble damped fluctuations. Most recently due to the fast advancement of power systems, design an optimal PSS by containing uncertainty is becoming to an essential issue. A novel sparse recursive least square algorithm to regulate the parameters of the PSS to damp fluctuations is presented in Ref. [23]. Also, the proposed controller has been applied to SMIB various disturbances. Nowadays, the control operations have given superior progress in the power system [24]. Fractional-order proportional-integral-derivative ($PI^\lambda D^\mu$) controller has received a major consideration in the last decade [25-27]. $PI^\lambda D^\mu$ calculus provides a novel mathematic module for the power system and prepares a complete mathematic model for complex systems [28]. A novel $PI^\lambda D^\mu$ controller designing method is presented in Ref. [29]. The optimal parameters of $PI^\lambda D^\mu$ controller are gained by reducing the integrated absolute error (IAE). In this paper, in order to optimize the efficiency of the power system, a

novel optimal controller design is characterized as an optimization tool and the Gray Wolf Optimization (GWO) algorithm is used to solve this problem. The GWO algorithm is one of the most best heuristic algorithms which were first presented by Mirjalili et al. in 2014 [30]. It can find a superior solution within a shorter time than other random algorithms. This paper purposes a novel optimal fuzzy based fractional order PID ($FPI^\lambda D^\mu$) controller, to optimize the parameters using the GWO algorithm. The GWO algorithm has been compared with the PSO in controller design [31]. The targets of this work are:

- An extensive dynamic model of PV power units has been extended to study small signal stability in power systems.
- A novel optimal $FPI^\lambda D^\mu$ controller is proposed for damping of fluctuations.
- The GWO algorithm is used to search for $FPI^\lambda D^\mu$ stabilizer parameters in the attendance of multi-machine system connected to PV unit.

The remainder of the study is organized as follows. In Section 2, precise component system modeling, including large scale PV and conventional units, used for low frequency studies, is introduced. In Section 3, the optimal method for designing a novel controller for the system incorporating PV unit is presented. Also, the tuned parameters for the stabilizers are provided in this part. Section 4 analyzes the time-domain results gained from the model and solution method. Finally, in Section 5, conclusions are given.

2. SYSTEM CONFIGURATION AND MODELS

In this study the influences of a power system, including multi-conventional generators and large scale PV unit on the low frequency oscillations of the power system are studied. To achieve the aim, various components of power system, including PV power unit, generators and their control systems must be first modeled. Figure 1 demonstrates the configuration of the studied large-size PV unit connected multi-machine power system. The system parameters have been provided in Ref [32] (without the PV unit). The details of PV parameters have been presented in the Appendix.

2.1. Models of converters and MPPT function

DC-DC boost convertor is employed because the PV output voltage level is low. The circuit of the DC-DC boost converter which connected to the PV power unit shown in Fig. 2. The mathematical equations of the converter can be obtained as follows [33]:

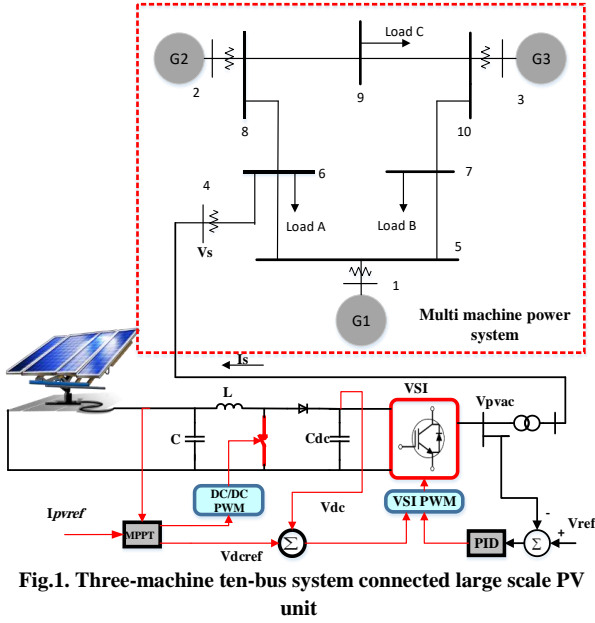


Fig. 1. Three-machine ten-bus system connected large scale PV unit

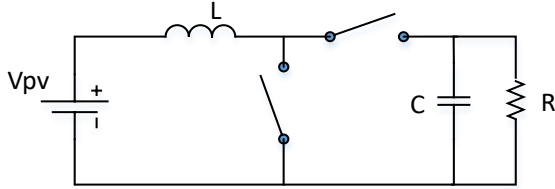


Fig. 2. Schematic of the DC-DC boost converter

$$\dot{i}_L = \frac{V_c \times d}{L} - \frac{V_C}{L} + \frac{V_{PV}}{L} \quad (1)$$

$$\dot{V}_C = \frac{i_L}{C} - \frac{d \times i_L}{C} - \frac{V_C}{RC} \quad (2)$$

Where, i_L is the DC-DC inductor current, d is the duty cycle, V_{PV} output voltage of the large-size PV unit and V_c is the DC-DC capacitor voltage.

The DC-DC boost converter in this work is equipped with a maximum power point tracking (MPPT) function which enables it to act as a MPPT controller for the PV unit. Hence, for DC-DC converter, we have:

$$d = d_0 + T_d (I_{pv-ref} - I_{pv}) \quad (3)$$

Where, I_{pv-ref} is the reference current of PV, d is the duty cycle, I_{pv} is the output current of PV and the transfer function of the PV current controller DC-AC inverter (T_d) is used to change the DC voltage to AC voltage for connecting to the power system. The AC voltage of inverter is given as follow [25]:

$$\bar{V}_{pvac} = mkV_{dc} (\cos \psi + j \sin \psi) \quad (4)$$

Where, k is generally equal to 0.75, ψ is the angle deviation between V_{pvac}^- and V_{dc} . The DC-AC inverter has two diverse controllers. ϕ is the phase of the pulse width modulation and m is the modulation rate.

$$\phi = \phi_0 + T_{vdc}(s)(V_{dc} - V_{dc-ref}) \quad (5)$$

$$m = m_0 + T_{vac}(s)(V_s - V_{s-ref}) \quad (6)$$

Where, T_{vdc} is DC voltage controller transfer function and T_{vac} is AC voltage controller transfer function. The equation of the DC-AC inverter can be obtained as [22]:

$$\dot{V}_{dc} = \frac{1}{C_{dc}} (I_{dc2} - I_{dc1}) \quad (7)$$

2.2. Dynamic model of PV power plant

Generally, large-size PV unit can be formed with four necessary components, PV cells, power electronic DC-AC inverter, DC-DC boost converter and the controllers associated with it [34, 35]. A PV array contains of PV modules that are connected in parallel-series template. The PV array with N_s modules in series and N_p in parallel is modeled. The model for PV that employed in this study is leaning on the single diode model. The tantamount model is shown in Fig 3. The current - voltage characteristic of the PV unit is:

$$V_{PV} = \frac{N_s n k T}{q} \ln \left(\frac{N_p I_{SC} I_r - I_{PV}}{N_p I_0} + 1 \right) \quad (8)$$

Where, I_r is the irradiance, T is the junction temperature, n is the ideality factor, N_p and N_s are the number of PV cells in parallel and series circuits, respectively. k is the Boltzmann's constant, I_{SC} is the short circuit current, q is the electron charge and I_0 is the saturation current.

It should be note that the light current I_{PV} has direct relationship with solar irradiance. With regard to the impacts of temperature and irradiance on light current, the light current approximated as follow:

$$I_r(G_a, T) = I_{SC} \frac{G_a}{G_{as}} [1 + \Delta I_{SC}(T - T_s)] \quad (9)$$

Where, T and G_a depute temperature and irradiance, respectively. Other parameters in Eq. (9) are constants: G_{as} is the standard irradiance ($1000w/m^2$), I_{sc} is the short circuit current, ΔI_{SC} is the temperature coefficient of short circuit current, and T_s is the standard temperature (298K). From Ref. [36], the saturation current I_0 can be obtained as:

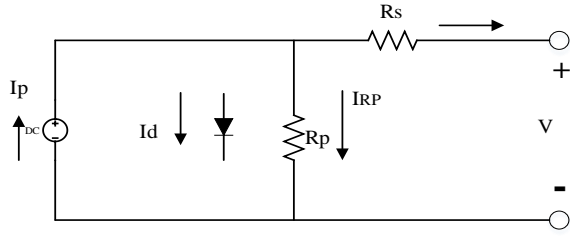


Fig. 3. The equivalent model for PV employed in this paper

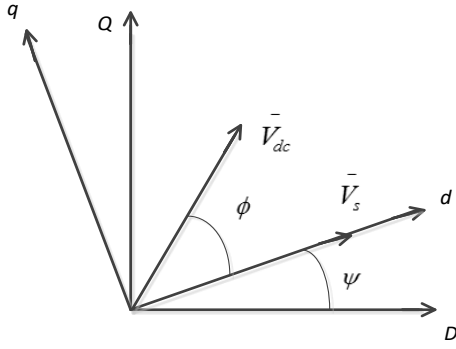


Fig. 4. $d-q$ axes Phasor diagram of the large scale PV unit

$$I_0(G_a, T) = \frac{I_r(G_a, T)}{\left[\exp\left(\frac{V_{OC}}{\alpha V_t}\right) - 1 \right]} \quad (10)$$

Where, $V_t = \frac{akT}{q}$ is the thermal voltage, α is the ideality factor and V_{OC} is the open circuit voltage.

2.3. Grid-connected PV unit

Figure 4 demonstrates $d-q$ phasor diagram of the PV power unit. Where, Q and D are the common system axes coordinates for all generators in the power system, q and d are the system individual system coordinate axes for the PV power unit [37].

With a little regard, it can be derived from Fig. 4 [38]:

$$\begin{bmatrix} I_{sD} \\ I_{sQ} \end{bmatrix} = \begin{bmatrix} \cos \varphi & -\sin \varphi \\ \sin \varphi & \cos \varphi \end{bmatrix} \begin{bmatrix} I_{sd} \\ I_{sq} \end{bmatrix} \quad (11)$$

$$I_{S_{D-Q}} = I_{S_{d-q}} e^{-j\varphi} \quad (12)$$

It is supposed that there are a large scale PV power unit and N machines in the power system. The matrix of the system admittance which reduced can be obtained as [37]:

$$Y_R = \begin{bmatrix} Y_M \\ Y_{PV} \end{bmatrix} \quad (13)$$

After simplification of Eq. (13), we have:

$$\begin{bmatrix} I_{Ma} \\ I_{PV} \end{bmatrix} = \begin{bmatrix} Y_{Ma, Ma} & Y_{Ma, PV} \\ Y_{PV, Ma} & Y_{PV, PV} \end{bmatrix} \begin{bmatrix} V_{Ma} \\ V_{PV} \end{bmatrix} \quad (14)$$

$$\begin{bmatrix} I_{Ma} \\ I_{PV} \end{bmatrix} = \begin{bmatrix} Y_G \\ Y_S \end{bmatrix} \begin{bmatrix} V_{Ma} \\ V_{PV} \end{bmatrix}$$

$$Y_G = \begin{bmatrix} Y_{Ma, Ma} & Y_{Ma, PV} \end{bmatrix} \quad (15)$$

$$Y_S = \begin{bmatrix} Y_{PV, Ma} & Y_{PV, PV} \end{bmatrix}$$

$$Y = \begin{bmatrix} Y_G \\ Y_S \end{bmatrix}$$

Where, $Y_{Ma, Ma}$ is $N \times N$, $Y_{PV, PV}$ is 1×1 and $Y_{Ma, PV}$ is $N \times 1$ matrices. From the Eq. (15) and the Eqs in Ref. [32], we have:

$$I_{Ma_i} = \sum_{n=1}^N Y_{G_{in}} \cdot [e^{j(90-\delta_n)} \cdot E'_{qn} + (x'_{qn} - x'_{dn}) \cdot e^{-j\delta_n} \cdot I_{qn}] \quad (16)$$

$i = 1, 2, \dots, N$

Where, δ is the torque angle, x'_d synchronous reactance of the transient state in q -axis and E'_q is internal voltage behind transient reactance. In $d_i - q_i$ coordinates:

$$i_i = I_i e^{j\delta_i} \quad (17)$$

$$i_i = \sum_{n=1}^N Y_{G_{in}} [e^{j(B_{in} + \delta_{in} + 90)} \cdot E'_{qn} + (x'_{qn} - x'_{dn}) \cdot e^{j(B_{in} + \delta_{in})} \cdot I_{qn}] \quad (18)$$

Where,

$$Y_{G_{in}} = Y_{in} e^{jB_{ni}} \quad , \quad \delta_{in} = \delta_i - \delta_n \quad (19)$$

Therefore,

$$i_{di} = \text{Re}(i_i), \quad i_{qi} = \text{Im}(i_i) \quad i = 1, 2, \dots, N \quad (20)$$

Now, the Y_S from Eq.(15) can be written as follows:

$$Y(z, n) = Y_{PV}(n) - \sum_{j=1}^N i \times [Y_{PV}(j) \times x'_d(j) \times Y_R(j, n)] \quad (21)$$

$z = N + 1$; PV location

$$n = 1, \dots, N + 1$$

Till now, this work derived the variables V_1, \dots, V_N of the modified matrix of the system admittance. Since the PV converter AC voltage of equals the following:

$$V = m k V_{dc} \sin(\psi) \quad (22)$$

$$\psi = \phi + \varphi$$

Therefore, i_d and i_q currents for all generators can

be written as follows:

$$\begin{aligned}
 i_{di} &= \sum_{n=1}^N Y_{in} [-\sin(B_{in} + \delta_{in}).E_{qn} \\
 &\quad + (x_{qn} - x'_{dn}).\cos(B_{in} + \delta_{in}).I_{qn}] \\
 &\quad + Y_{iz} m k V_{dc} \cos(\psi + \delta_i) \\
 i_{qi} &= \sum_{n=1}^N Y_{in} [\cos(B_{in} + \delta_{in}).E_{qn} \\
 &\quad + (x_{qn} - x'_{dn}).\sin(B_{in} + \delta_{in}).I_{qn}] \\
 &\quad + Y_{iz} m k V_{dc} \cos(\psi + \delta_i) \\
 i &= 1, \dots, N \\
 z &= N + 1 \quad ; PV \text{ location}
 \end{aligned} \tag{23}$$

PV current in $d_i - q_i$ axes can be obtained by the Eqs. (21) and (22). That is written as follows:

$$I_S = \sum_{n=1}^{N+1} Y_{S_n} V_n e^{-\varphi} \tag{24}$$

As, we have:

$$\begin{aligned}
 I_{Sd} &= \text{Re}(I_S) \\
 I_{Sq} &= \text{Im}(I_S)
 \end{aligned} \tag{25}$$

2.4. Complete linearized network model

In this part, the power system demonstrated in Figure 1 is linearized. We can linearize a nonlinear system by considering the low disturbance about a working point. At first, to linearize the system, the initial conditions must be found by a power flow tools. For linearization of the power system, we applied the method in [32].

$$\Delta(i_{di} + j i_{qi}) = \Delta I_{di} + j \Delta I_{qi} \tag{26}$$

See more details in Appendix A.

Linearization of the PV unit (Eqs. (8) and (9)) around the balance point can be obtained as:

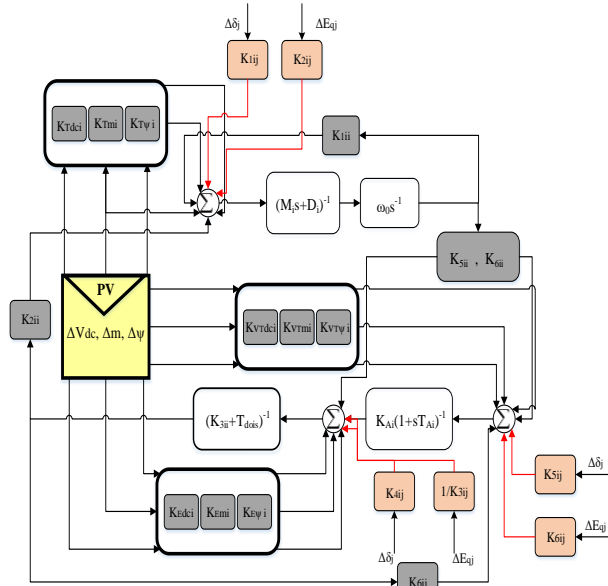


Fig. 5. A small signal model of a large size PV unit installed to the

multi-machine power system

$$\Delta V_{PV} = \frac{N_S n K T}{q} \left(\begin{aligned} &\left(\begin{aligned} &\left[\frac{\Delta I_{PV}}{N_P I_0} \right] \\ &- \frac{I_{SC} I_0 + I_{PV0}}{100 I_0 + N_P I_0} + 1 \end{aligned} \right) \\ &+ \left(\begin{aligned} &\frac{I_{SC} \Delta I_r}{100 I_0} \\ &+ \frac{I_{SC} I_0 + I_{PV0}}{100 I_0 + N_P I_0} + 1 \end{aligned} \right) \end{aligned} \right) \tag{27}$$

$$\Delta I_r = I_{SC} \frac{G_a}{G_n} \Delta I_{SC} \Delta T \tag{28}$$

$$\Delta T = T - T_s \tag{29}$$

Eventually, linearization of the system can be shown as:

$$\dot{\Delta \delta}_i = \omega_{i0} \Delta \omega_i \tag{30}$$

$$\dot{\Delta \omega}_i = \frac{1}{M_i} \begin{pmatrix} -K_{1i} \Delta \delta_i - D_i \Delta \omega_i \\ -K_{2i} \Delta E'_{qi} - K_{TVdc} \Delta V_{dc} \\ -K_{Tmi} \Delta m - K_{T\psi} \Delta \psi \end{pmatrix} \tag{31}$$

$$\dot{\Delta E'_{qi}} = \frac{1}{T_{d0i}} \begin{pmatrix} -K_{4i} \Delta \delta_i - K_{3i} \Delta E'_{qi} \\ -K_{EVdc} \Delta V_{dc} - K_{Em} \Delta m \\ -K_{E\psi} \Delta \psi + \Delta E'_{fdi} \end{pmatrix} \tag{32}$$

$$\begin{aligned}
 \dot{\Delta E'_{fdi}} &= -\frac{1}{T_{Ai}} \Delta E'_{fdi} \\
 &- \frac{K_{Ai}}{T_{d0i}} \begin{pmatrix} K_{5i} \Delta \delta_i + K_{6i} \Delta E'_{qi} \\ + K_{VTdc} \Delta V_{dc} + K_{VTm} \Delta m \\ + K_{VT\psi} \Delta \psi \end{pmatrix}
 \end{aligned} \tag{33}$$

By using of the Eqs (30-33), the diagram for i^{th} generator can be demonstrated in Fig. 5.

3. SYSTEM CONTROL AND OPTIMIZATION

3.1. Structure of $FPI^\lambda D^\mu$ based stabilizers

To ameliorate the efficiency and robustness of PID controller, Podlubny has presented $PI^\lambda D^\mu$ controller because of including an integrator of the order λ and differentiator of order μ . This control system is formulated in [23]. The Riemann-Liouville (RL) definition for the $PI^\lambda D^\mu$ controller can be written as follows:

$$\alpha D_t^\alpha F(t) = \frac{1}{\Gamma(n-\alpha)} \left(\frac{d}{dt} \right)^n \int_0^t \frac{f(\tau)}{(t-\tau)^{1-(n-\alpha)}} dt \tag{34}$$

$\Gamma(0)$ is the Gamma function of Euler that determines

the allocates and factorial operator, to obtain non-integer values. An alternative definition, based on the indication of fractional differentiation, which is the Grunwald-Letnikov expression has illustrated the following:

$$\begin{aligned} \alpha D_t^\alpha F(t) &= \lim_{g \rightarrow 0} \left(\frac{1}{\Gamma(\alpha) g^\alpha} \right) \\ &\times \sum_{d=0}^{(t-\alpha)/g} \frac{\Gamma(\alpha+d)}{\Gamma(g+d)} f(t-dg) \end{aligned} \quad (35)$$

The function of $PI^\lambda D^\mu$ controller is acquired through Laplace transform and is obtained as:

$$U_{PI^\lambda D^\mu}(s) = (K_P + K_I s^{-\lambda} + K_D s^\mu) \Delta \omega \quad (36)$$

Fuzzy logic control (FLC) employed as an input signal for $PI^\lambda D^\mu$ controller to reduce and damp the oscillations as created by disturbance. We applied the proposed $PI^\lambda D^\mu$ controller in all generators (G1,G2,G3). The structure of $FPI^\lambda D^\mu$ stabilizer is shown in Fig. 6.

The FLC inputs are the angle deviation ($\Delta \delta$) and speed deviation ($\Delta \omega$). On the other hand the output produces the signal for $PI^\lambda D^\mu$ controller. The aim of the controller is to ameliorate the damping of the fluctuations because of perturbations of the power system. The speed deviation ($\Delta \omega$), angle deviation ($\Delta \delta$) and the output signal of FLC (O) are divided into seven membership functions with limited area $[-0.8, 0.8]$. Figure 7 illustrates these membership functions [16]. The rules of FLC designed by past experience of the controlled system are demonstrated in Table 1.

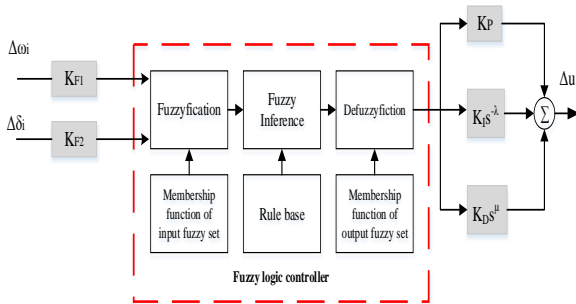


Fig. 6. Structure of $FLPI^\lambda D^\mu$ stabilizer

Table 1. Rules for the FLC

$\Delta \delta \backslash \Delta \omega$	NB	NM	NS	ZE	PS	PM	PB
NB	ONB	ONB	ONB	ONB	ONS	ONS	OZE
NM	ONB	ONB	ONM	ONM	ONS	OZE	OPS
NS	ONB	ONM	ONM	ONS	OZE	OPS	OPM
ZE	ONM	ONM	ONS	OZE	OPS	OPM	OPM
PS	ONM	ONS	OZE	OPS	OPM	OPM	OPB
PM	ONS	OZE	OPS	OPM	OPM	OPB	OPB
PB	OZE	OPS	OPM	OPB	OPM	OPB	OPB

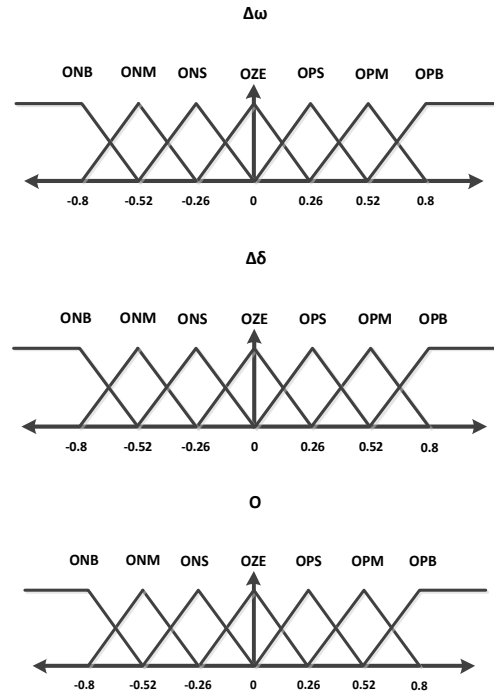


Fig. 7. Membership function of FLC

Designing of $FPI^\lambda D^\mu$ controller requires to tune the following parameters: $K_P, K_D, K_I, KF_1, KF_2$ and μ, λ which are the proportional, differential, integral, Fuzzy coefficients constants, fractional order integral and derivative elements respectively.

3.2. A brief description of GWO algorithm

The GWO method is one of the latest bio-inspired algorithm was introduced by Mirjalili et al., in 2014 [30]. There are four categories of these wolves: alpha (α), delta (δ), beta (β) and omega (ω), in decreasing order of dominance. In every iteration, Beta, Alpha and Delta wolves update their position according to position of prey. These updates will continue until the distance between prey stop moving or satisfactory result is met. α is the best solution in modeling of these wolves. Every other wolf surpasses its dominance. The hunting is mainly guided by α , and β , then δ and followed by the ω . The first step is surrounding the prey and mathematically it is given as Eqns. (37) and (38).

$$\vec{D} = \left| \vec{C} \cdot \vec{X}_p(t) - \vec{X}(t) \right| \quad (37)$$

$$\vec{X}(t+1) = \vec{X}_p(t) - \vec{A} \cdot \vec{D} \quad (38)$$

$$\vec{A} = 2 \cdot a \cdot r_1 - a \quad (39)$$

$$\vec{C} = 2 \cdot r_2 \quad (40)$$

Where, t indicates the iterations, C and A indicate the

coefficient vectors, X_p is the prey position and X is the wolf position of the grey wolf. The parameter of a decreases from 2 to 0 linearly over every iteration and $r1$ and $r2$ are random number within $[0,1]$. Alpha (α), Beta (β), and Delta (δ), three best solution chosen first and update their position of other agents pursuant to the best search solution. The mathematical equation for this solution is [30]:

$$\vec{D}_\alpha = \left| \vec{C}_1 \cdot \vec{X}_\alpha - \vec{X} \right|$$

$$\vec{D}_\beta = \left| \vec{C}_2 \cdot \vec{X}_\beta - \vec{X} \right|$$

$$\vec{D}_\delta = \left| \vec{C}_3 \cdot \vec{X}_\delta - \vec{X} \right|$$
(41)

$$\vec{X}_1 = \vec{X}_\alpha - A_1 \cdot \vec{D}_\alpha$$

$$\vec{X}_2 = \vec{X}_\beta - A_2 \cdot \vec{D}_\beta$$

$$\vec{X}_3 = \vec{X}_\delta - A_3 \cdot \vec{D}_\delta$$
(42)

$$\vec{X}(t+1) = \frac{\vec{X}_1 + \vec{X}_2 + \vec{X}_3}{3}$$
(43)

Alpha, Beta, and Delta wolves encompassed around the prey and update their position within the circle. The Flowchart of gray wolf optimization is shown in Fig. 8.

3.3. $FPI^{\lambda D^\mu}$ Controller based GWO

After linearizing the system, the eigenvalues of the system are calculated, and the desired objective function can be formulated using only the slightly damped or unstable electromechanical modes that require to be shifted. The objective function for GWO to tuning of the parameters of controller is defined by the following:

$$OF = \text{Min} \left(\text{Max} \left(\text{Re}_i \right) + \sum_{j=1}^n (1 - \xi_j) \right)$$

$$i = 1, 2, \dots, n$$
(44)

Where, n is the full number of the eigenvalues, Re is the real of eigenvalues and ξ_j is the damping ratio. As regards, in every iteration of optimization algorithm, there are some Eigen values, so we should choose the worst one (the maximum one) and also we should calculate all damping rate (in this equation, being close to zero is better). Therefore, we should choose the minimum one in all iteration. The constraints on the controller parameter are defined Eq. 45.

Typical limited areas of the parameters are $[0.001-4]$ for K_P, K_I, K_D , $[0.001-1]$ for λ, μ and $[1-20]$ for KF_1 and KF_2 .

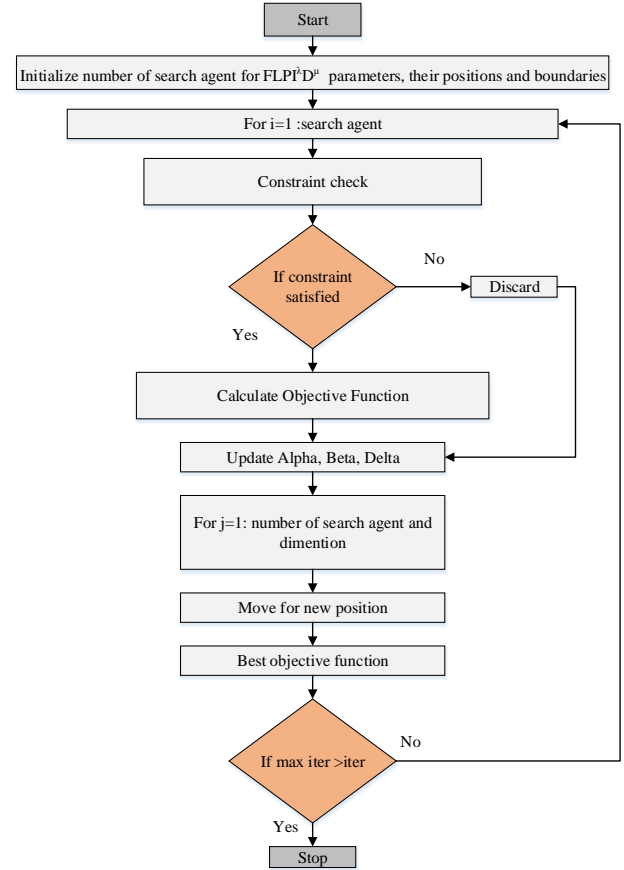


Fig. 8. A flowchart of GWO algorithm

$$K_I^{\min} \leq K_I \leq K_I^{\max}, \quad K_P^{\min} \leq K_P \leq K_P^{\max}$$

$$K_D^{\min} \leq K_D \leq K_D^{\max}, \quad \lambda^{\min} \leq \lambda \leq \lambda^{\max}$$

$$\mu^{\min} \leq \mu \leq \mu^{\max}, \quad KF_1^{\min} \leq KF_1 \leq KF_1^{\max}$$

$$KF_2^{\min} \leq KF_2 \leq KF_2^{\max}$$
(45)

4. SIMULATION AND DISCUSSION

Three scenarios will be considered to appraise the small signal modeling of the large scale PV connecting multi-machine system and proposed controller (Table 2).

Table 3 demonstrates the optimized values of the parameters using GWO for the $FPI^{\lambda D^\mu}$ controller.

Table 2. Considered scenarios

Scenario	P_{PV}	P_{G2}	P_{G3}
Scenario 1	0.3 pu	1.63 pu	0.85 pu
Scenario 2	0.7 pu	1.43 pu	0.65 pu
Scenario 3	1.2 pu	1.13 pu	0.45 pu

Table 3. Optimal $FPI^{\lambda D^\mu}$ controller based GWO parameters

Parameters	KF_1	KF_2	K_P	K_I	K_D	μ	λ
Optimal value	24.5	10.58	3.99	1.75	2.52	0.84	0.16

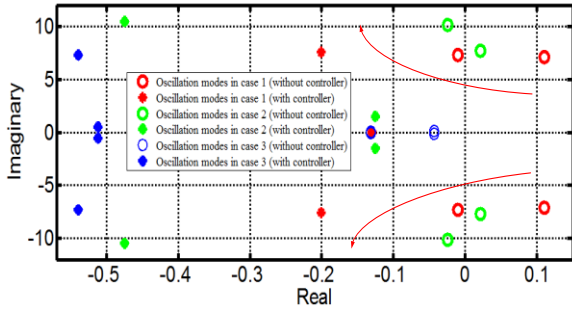


Fig. 9. Oscillation modes of the system in three scenarios

To display the intensive performance of the tuned $FPI^{\lambda}D^{\mu}$ controller, the oscillation modes gained in three scenarios, both without and with $FPI^{\lambda}D^{\mu}$ controller are shown in Fig. 9. The analysis proves that the low-frequency eigenvalues near the imaginary axis are the most superior and obligatory for system stability, while the eigenvalues close to the real axis will affect the dynamic performance. It is obvious that some of the eigenvalues are in an unstable area (the positive part of real axis) and in some scenarios, are weakly damped, When the controller is not installed. Although, it can be concluded that the power system has an oscillation which must be solved it. It is also obvious that the dynamic stability of the power system with the novel controller is significantly improved. The results show the system stability can be affected either positively or negatively by the PV power unit when system conditions change. In this study, the performance of the proposed stabilizer under transient conditions is verified by applying a step input signal.

Scenario 1: In this part, the efficiency of the $FPI^{\lambda}D^{\mu}$ controller under different conditions is confirmed. The output responses of the system as demonstrated in Figs. 10, 11 confirm that system is unstable. In this scenario, the PV power is lower than all the generators in the system. Figures 10, 11 display the plot of speed deviations between generator G1 and G2, G3 of the equipped generators with different controller under the perturbation.

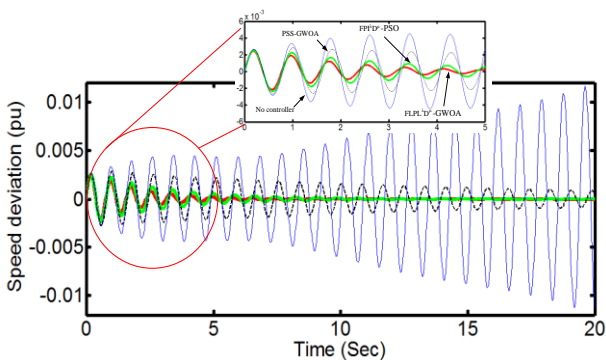


Fig.10. Speed deviation among conventional generator G1 and G2 with different controllers in scenario 1

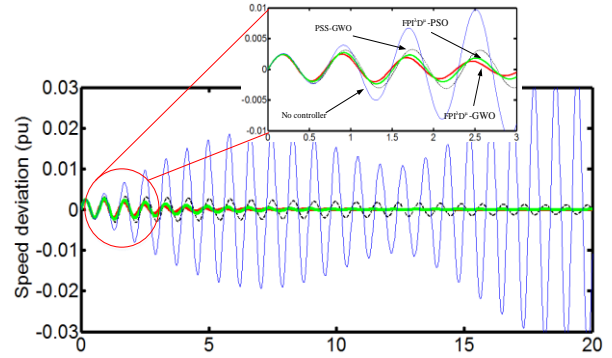


Fig.11. Speed deviation among conventional generator G1 and G3 with different controllers in scenario 1

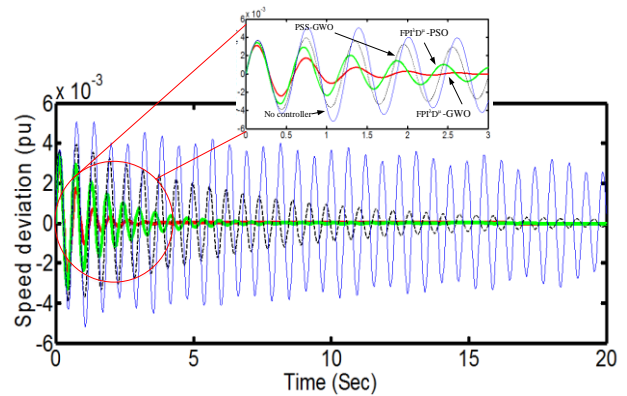


Fig.12. Speed deviation among conventional generator G1 and G2 with different controllers in scenario 2

By inspection of the curves in Figures 10 and 11, it is noticed that the speed deviation of the power system which used $FPI^{\lambda}D^{\mu}$ controller based GWO reached a superior damping against another stabilizer.

Scenario 2: In this case, the PV power injected into the power network is lower than the power supplied from one generator in the system and more than from two remained generators to the grid. The efficiency of the power system in this scenario is similar the scenario 1, therefore the power system without controller will be instable. The speed deviations between generator G1 and G2, 3of the power system with various controllers in this case are illustrated in Figures 12 and 13. The system fluctuations are damped with the optimal $FPI^{\lambda}D^{\mu}$ controller which proves the eigenvalue analysis. It is obvious that when the power system has a controller, it will be stable with proper damping factors. In this scenario, also the $FPI^{\lambda}D^{\mu}$ controller based GWO achieved a better damping than the other controller.

Scenario 3: In this section, the PV power penetrated into the power system is more than the power generated from all the conventional generators in the system. It is obvious that the performance of the network is preferable than the other scenarios and eventually, the system will be stable with short time.

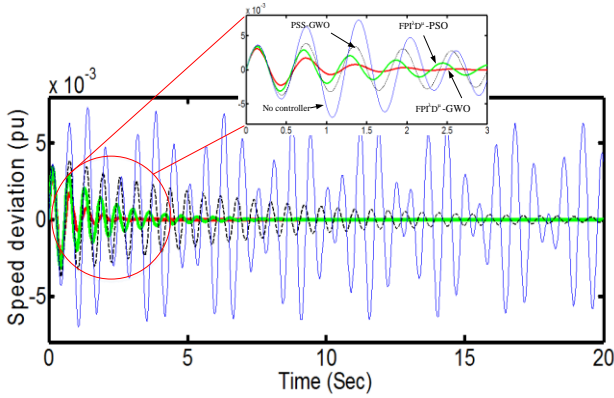


Fig.13. Speed deviation among conventional generator G1 and G3 with different controllers in scenario 2

The speed deviations between generator G1 and G2, 3 of the system with various controllers are demonstrated in Figures 14 and 15. The speed deviation system with $FPI^{\lambda}D^{\mu}$ controller based GWO is superior than that with GWO based conventional PSS with less overshoot and settling time.

To demonstrate performance robustness of the proposed method, the Integral of the Time multiplied Absolute value of the Error (ITAE) is defined as:

$$ITAE = 1000 \int_0^{t_{sim}} t. (|w_1 - w_2| + |w_1 - w_3|) dt \quad (46)$$

Where, w_1, w_2, w_3 are the speed rotors of generator G1, G2 and G3, respectively. It is worth mentioning that the lower the value of this indice is, the better the system response in terms of time-domain characteristics. Numerical results of performance robustness for all cases are listed in Table 4. It can be seen that the values of this index with the $FPI^{\lambda}D^{\mu}$ controller based GWO are much smaller compared to that PSS-GWO and $FPI^{\lambda}D^{\mu}$ -PSO.

Table 4: Numerical results of ITAE index for all cases

Method	ITAE		
	Scenario 1	Scenario 2	Scenario 3
PSS-GWO	78.21	69.48	37.12
$FPI^{\lambda}D^{\mu}$ -PSO	11.63	28.04	13.92
$FPI^{\lambda}D^{\mu}$ -GWO	10.04	14.46	7.39

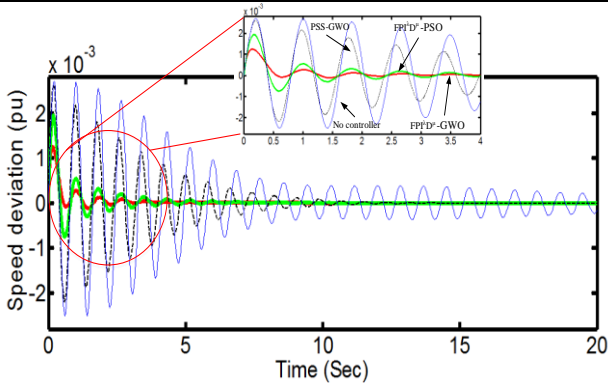


Fig.14. Speed deviation among conventional generator G1 and G2 with different controllers in scenario 2

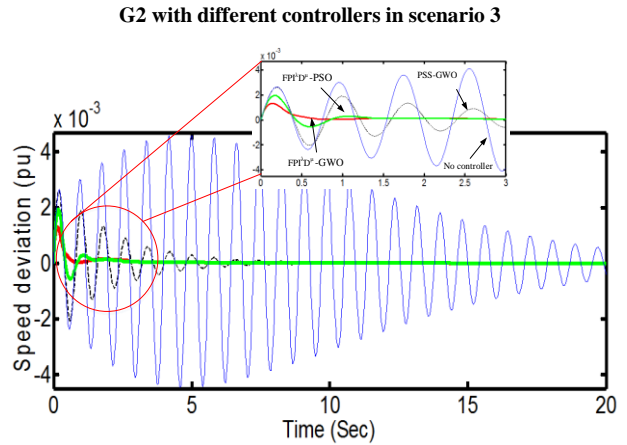


Fig.15. Speed deviation among conventional generator G1 and G3 with different controllers in scenario 3

5. CONCLUSIONS

High penetration of large scale PV unit compared with conventional generators makes an increased responsibility on power system planners related to studying its effect on dynamic grid. In this study, a novel technique for small signal modeling of conventional multi-machine power system with the large scale PV unit is presented due to study small signal stability in power systems. Also, a novel $FPI^{\lambda}D^{\mu}$ controller is presented for debilitate the oscillations of imported perturbation in the system in attendance of a PV power plant. The tuned parameters of the $FPI^{\lambda}D^{\mu}$ controller are done. To obtain the optimized parameters, the GWO method is employed to solve the problem. The comparison between GWO and PSO results illustrates the effectiveness of application of the GWO algorithm to optimize the controller. Simulation study in the multi-machine connected to the large scale PV unit proves that the stabilizing consequence of the system with $FPI^{\lambda}D^{\mu}$ controller based GWO are much premiere to those of the classic PSS.

Appendix A.

From Eq. (26), we will have:

$$\begin{aligned}
 [\Delta I_d] &= [P_d][\Delta \delta] + [Q_d][\Delta E_q] + [M_d][\Delta I_q] \\
 &\quad + [dvdcd][\Delta V_{dc}] + [dmd][\Delta m] + [dsayd][\Delta \psi] \\
 [L_q][\Delta I_q] &= [P_q][\Delta \delta] + [Q_q][\Delta E_q] + [dvdcq][\Delta V_{dc}] \\
 &\quad + [dmq][\Delta m] + [dsayq][\Delta \psi]
 \end{aligned} \quad (A-1)$$

Where,

$$\begin{aligned}
 P_{dij} &= -|Y_{Gij}| [\cos(B_{ij} + \delta_{ij}) \\
 &\quad + (x_{qj} - x'_{dij}) \times \sin(B_{ij} + \delta_{ij}) \times I_{qj}]
 \end{aligned} \quad (A-2)$$

$i \neq j$

$$P_{qij} = -|Y_{Gij}|[\sin(B_{ij} + \delta_{ij}) - (x_{qj} - x'_{dj}) \times \cos(B_{ij} + \delta_{ij}) \times I_{qj}] \quad (A-3)$$

$$P_{dii} = -\sum_{i \neq j} P_{dij} - [Y_{iz} \times m_0 \times k \times V_{dc0} \times \sin(\delta_{0i} + \psi_0)] \quad (A-4)$$

$$P_{qii} = -\sum_{i \neq j} P_{qij} - [Y_{iz} \times m_0 \times k \times V_{dc0} \times \cos(\delta_{0i} + \psi_0)] \quad (A-5)$$

z : PV location

$$Q_{dij} = -Y_{Gij} \times \sin(B_{ij} + \delta_{ij}) \quad (A-6)$$

$$Q_{qij} = Y_{Gij} \times \cos(B_{ij} + \delta_{ij}) \quad (A-7)$$

$$L_{qij} = -|Y_{Gij}|(x_{qij} - x'_{dj}) \times \sin(B_{ij} + \delta_{ij}) \quad (A-7)$$

$$L_{qii} = 1 - |Y_{Gij}|(x_{qij} - x'_{dj}) \times \sin(B_{ij} + \delta_{ij}) \quad (A-8)$$

$$M_{dij} = -|Y_{Gij}|(x_{qij} - x'_{dj}) \times \cos(B_{ij} + \delta_{ij}) \quad (A-8)$$

$$i = 1, \dots, N \quad j = 1, \dots, N$$

$$dvdc d_i = Y_{iz} \times m_0 \times k \times \cos(\psi_0 + \delta_i) \quad (A-9)$$

$$dmd_i = Y_{iz} \times V_{dc0} \times k \times \cos(\psi_0 + \delta_i) \quad (A-9)$$

$$dsay d_i = -Y_{iz} \times V_{dc0} \times m_0 \times k \times \sin(\psi_0 + \delta_i) \quad (A-10)$$

$$dvdc q_i = Y_{iz} \times m_0 \times k \times \sin(\psi_0 + \delta_i) \quad (A-10)$$

$$dmq_i = Y_{iz} \times V_{dc0} \times k \times \sin(\psi_0 + \delta_i) \quad (A-10)$$

$$dsay q_i = Y_{iz} \times V_{dc0} \times m_0 \times k \times \cos(\psi_0 + \delta_i) \quad (A-10)$$

$$z = N + 1 \quad ; SOFC \text{ location}$$

For the calculation of all $P, Q, L, M, dvdc, dm, dsay$ coefficients, initial values should be used. The solutions of $[\Delta I_d]$ and $[\Delta I_q]$ of Eq. (45) can be formulated as:

$$\begin{aligned} [\Delta I_d] &= [Y_d][\Delta E_q] + [F_d][\Delta \delta] \\ &+ [DVDCd][\Delta V_{dc}] + [Dmd][\Delta m] \\ &+ [DSAYd][\Delta \psi] \\ [\Delta I_q] &= [Y_q][\Delta E_q] + [F_q][\Delta \delta] \\ &+ [DVDCq][\Delta V_{dc}] + [Dmq][\Delta m] \\ &+ [DSAYq][\Delta \psi] \end{aligned} \quad (A-11)$$

Where,

$$\begin{aligned} Y_q &= [L_q]^{-1}[Q_q], \quad Y_d = [Q_d] + [M_d][Y_q] \\ F_q &= [L_q]^{-1}[P_q], \quad F_d = [P_d] + [M_d][F_q] \\ DVDCd &= [M_d][DVDCq] + [dvdc d] \\ DVDCq &= [L_q]^{-1}[dvdc q] \\ Dmd &= [M_d][Dmq] + [dmd] \\ Dmq &= [L_q]^{-1}[dmq] \\ DSAYd &= [M_d][DSAYq] + [dsay d] \\ DSAYq &= [L_q]^{-1}[dsay q] \end{aligned} \quad (A-12)$$

The Heffron-Philips coefficients are obtained in the following:

$$K_{1ij} = D_t F_{dij} + Q_t F_{qij} \quad (A-13)$$

$$K_{2ii} = D_t Y_{dii} + Q_t Y_{qii} + I_{qi0} \quad (A-13)$$

$$K_{2ij} = D_t Y_{dij} + Q_t Y_{qij} \quad (A-13)$$

$$K_{Tvdxi} = Q_t DVDCq_i + D_t DVDCd_i \quad (A-14)$$

$$K_{Tmi} = Q_t Dmq_i + D_t Dmd_i \quad (A-14)$$

$$K_{T\psi i} = Q_t DSAYq_i + D_t DSAYd_i \quad (A-14)$$

$$K_{3ii} = [1 + [x_{di} - x'_{di}]Y_{dii}]^{-1} \quad (A-15)$$

$$K_{3ij} = [[x_{di} - x'_{di}]Y_{dij}]^{-1} \quad i \neq j \quad (A-15)$$

$$K_{4ij} = [x_{di} - x'_{di}][F_{dij}] \quad (A-15)$$

$$K_{Evdci} = [x_{di} - x'_{di}][DVDCd] \quad (A-16)$$

$$K_{Emi} = [x_{di} - x'_{di}][Dmd] \quad (A-16)$$

$$K_{E\psi i} = [x_{di} - x'_{di}][DSAYd] \quad (A-16)$$

$$[K_5] = [D_v][x_q][F_q] - [Q_v][x'_d][F_d] \quad (A-17)$$

$$[K_6] = [D_v][x_q][Y_q] - [Q_v][x'_d][Y_d] + [Q_v] \quad (A-17)$$

$$[K_{VTdc}] = [D_v][x_q][DVDCq] - [Q_v][x'_d][DVDCd] \quad (A-18)$$

$$[K_{VTm}] = [D_v][x_q][Dmq] - [Q_v][x'_d][Dmd] \quad (A-18)$$

$$[K_{VT\psi}] = [D_v][x_q][DSAYq] + [Q_v][x'_d][DSAYd] \quad (A-18)$$

$$D_t = (x_{qi} - x'_{di})I_{qi0} \quad (A-19)$$

$$Q_t = (x_{qi} - x'_{di})I_{di0} + E_{qi0} \quad (A-19)$$

$$[D_v] = [V_{t0}]^{-1}[V_{d0}] \quad (A-19)$$

$$[Q_v] = [V_{t0}]^{-1}[V_{q0}] \quad (A-19)$$

PV parameters are given as follows:

$I_0=4.66$	$V_{oc}=22v$	$I_{sc}=5$
$N_s=300$	$N_p=300$	$K=1.38065e-23$
$T_s=25 \text{ C}$	$G_n=1000 \text{ W/m}^2$	$I_{pv0}=2.996$
$K_v=0.346$	$\Delta I_{sc}=0.057$	$\eta=0.3$

Acknowledgement

The author gratefully acknowledges the JOAPE journal editorial board for their work on the original version of this document.

REFERENCES

- [1] R. Sen and SC. Bhattacharyya, "Off-grid electricity generation with renewable energy technologies in India: An application of HOMER", *Renewable Energy*, vol.62, pp. 388-398, 2014.
- [2] B. Vick and L. Almas, "Developing wind and/or solar powered crop irrigation systems for the great plains", *Appl. Eng. Agric.*, vol. 27, pp. 235-245, 2011.
- [3] F. Chueco-Fernández and A. Bayod-Rújula, "Power supply for pumping systems in northern Chile: Photovoltaics as alternative to grid extension and diesel engines", *Energy*, vol. 35, pp. 2909-2921, 2010.
- [4] O. Ellabana, H. Abu-Rubb and F. Blaabjerg,

- “Renewable energy resources: Current status, future prospects and their enabling technology”, *Renew. Sustain. Energy Rev.*, vol. 39, pp. 748-764, 2014.
- [5] R. Amini, A. Safari and S. Najafi, “Optimal model of PDIG based microgrid and design of complementary stabilizer using ICA”, *ISA Trans.*, vol. 64, pp. 328-341, 2016.
- [6] H. Chen and C. Pang, “Organizational forms for knowledge management in photovoltaic solar energy industry”, *Knowledge-Based Syst.*, vol. 23, pp. 924-933, 2010.
- [7] B. Tamimi, C. Cañizares and K. Bhattacharya, “System stability impact of large-scale and distributed solar photovoltaic generation: The case of Ontario, Canada”, *IEEE Trans. sustainable energy*, vol. 4, pp. 680-8, 2013.
- [8] L. Wang and T. Lin, “Dynamic stability and transient responses of multiple grid-connected PV systems”, *Transm. Distrib. Conf. Exposition*, 2008.
- [9] Y. Hashemi, H. Shayeghi, M. Moradzadeh and A. Safari, “Design of hybrid damping controller based on multi-target gravitational search optimization algorithm in a multi-machine power system with high penetration of PV park”, *J. Cent. South Univ.*, vol. 23, pp. 1163-75, 2016.
- [10] S. Eftekharnejad, V. Vittal, G. Heydt, B. Keel and J. Loehr, “Small signal stability assessment of power systems with increased penetration of photovoltaic generation: A case study”, *IEEE Trans. Sustainable Energy*, vol. 4, pp. 960-67, 2013.
- [11] Y. Liu, J. Bebic, B. Kroposki, J. De Bedout and W. Ren, “Distribution system voltage performance analysis for high-penetration PV”, *Energy 2030 Conf.*, 2008.
- [12] M. Zeraati, M. Golshan and J. Guerrero, “Distributed control of battery energy storage systems for voltage regulation in distribution networks with high PV penetration”, *IEEE Trans. Smart Grid*, vol. 9, pp. 3582-93, 2018.
- [13] M. Islam, M. Nadarajah and J. Hossain, “Short-term voltage stability enhancement in residential grid with high penetration of rooftop PV units”, *IEEE Trans. Sustainable Energy*, vol. 10, pp. 2211-22, 2018.
- [14] M. Pokharel, A. Ghosh and C. Ho, “Small-signal modeling and design validation of PV-controllers with INC-MPPT using CHIL”, *IEEE Trans. Energy Convers.* Vol. 34, pp. 361-371, 2018.
- [15] F. Selwa, L. Djamel and L. Imen, “influence of high pv penetration and STATCOM on rotor angle stability of SMIB transmission system”, *J. Electr. Eng. Technol.*, vol. 13, pp. 849-57, 2018.
- [16] Y. Zhang, C. Mensah-Bonsu, P. Walke, S. Arora and J. Pierce, “Transient over-voltages in high voltage grid-connected PV solar interconnection”, *Power Energy Soc. Gen. Meeting*, 2010.
- [17] A. Mohamed, A. Berzoy and O. Mohammed, “Design and hardware implementation of FL-MPPT control of PV systems based on GA and small-signal analysis” *IEEE Trans. Sustainable Energy*, vol. 8, pp. 279-90, 2017.
- [18] H. Setiadi, A. Krismanto and N. Mithulananthan, “Influence of BES system on local and inter-area oscillation of power system with high penetration of PV plants” *Appl. Syst. Innovation Int. Conf.*, 2017.
- [19] H. Liu, L. Jin, D. Le and A. Chowdhury, “Impact of high penetration of solar photovoltaic generation on power system small signal stability”, *Power Syst. Technol. Int. Conf.*, 2010.
- [20] B. Tamimi, C. Cañizares and K. Bhattacharya, “Modeling and performance analysis of large solar photovoltaic generation on voltage stability and inter-area oscillations.” *Power Energy Soc. Gen Meeting*, 2011.
- [21] W. Du, H. Wang and L. Xiao, “Power system small-signal stability as affected by grid-connected photovoltaic generation.” *Eur. Trans. Electr. Power*, vol. 22, pp. 688-703, 2012.
- [22] H. Shahsavari, A. Safari and J. Salehi, “Dynamic Analysis and Optimal Design of FLPSS for Power Network Connected Solid Oxide Fuel Cell Using of PSO” *J. Oper. Autom. Power Eng.*, vol. 5, pp. 215-25, 2017.
- [23] A. Safari, H. Shahsavari and F. Babaei, “Optimal design of controllers for power network connected sofc using of multi-objective PSO”, *Serbian J. Electr. Eng.*, vol. 15, pp. 145-163, 2018.
- [24] F. Babaei and A. Safari, “SCA based Fractional-order PID Controller Considering Delayed EV Aggregators.” *J. Oper. Autom. Power Eng.*, In Press, 2019.
- [25] I. Podlubny, “Fractional-order systems and PI/sup/spl lambda/D/sup/spl mu/-controllers”, *IEEE Trans. Autom. Control*, vol. 44, pp. 208-14, 1999.
- [26] R. Bouiadjra, M. Sedraoui and A. Younsi, “Robust fractional PID controller synthesis approach for the permanent magnetic synchronous motor.” *Int. J. Mach. Learn. Cyber.* vol. 9, pp. 2027-2041, 2018.
- [27] M. Moradi, “A genetic-multivariable fractional order PID control to multi-input multi-output processes.” *J. Process Control*, vol. 24, pp. 336-43, 2014.
- [28] B. Saidi, M. Amairi, S. Najjar and M. Aoun, “Bode shaping-based design methods of a fractional order PID controller for uncertain systems”, *Nonlinear Dyn.*, vol. 80, pp. 1817-38, 2015.
- [29] X. Li, Y. Wang, N. Li, M. Han, Y. Tang and F. Liu, “Optimal fractional order PID controller design for automatic voltage regulator system based on reference model using particle swarm optimization.” *Int. J. Mach. Learn. Cybern.*, vol. 8, pp. 1595-605, 2017.
- [30] S. Mirjalili, M. Mirjalili and A. Lewis, “Grey wolf optimizer”, *Adv. Eng. Software*, vol. 69, pp. 46-61, 2014.
- [31] A. El-Zonkoly, A. Khalil and N. Ahmied, “Optimal tuning of lead-lag and fuzzy logic power system stabilizers using particle swarm optimization”, *Expert Syst. Appl.* Vol. 36, pp. 2097-106, 2009.
- [32] A. Safari, H. Shahsavari and J. Salehi, “A mathematical model of SOFC power plant for dynamic simulation of multi-machine power systems”, *Energy*, vol. 149, pp. 397-413, 2018.
- [33] L. Wang, Q. Vo and A. Prokhorov, “Dynamic stability analysis of a hybrid wave and photovoltaic power generation system integrated into a distribution power grid”, *IEEE Trans. Sustainable Energy*, vol. 8, pp. 404-13, 2017.
- [34] H. Shahsavari and A. Safari, “Optimal design of novel FLPSS for power network connected solid oxide fuel cell using of HSS algorithm”, *Int.J. Energy Stat.*, vol. 5, 2017.
- [35] D. Lorente, S. Pedrazzi, G. Zini, A. Dalla and P. Tartarini, “Mismatch losses in PV power plants”, *Solar Energy*, vol. 100, pp. 42-49, 2014.
- [36] W. Xiao, W. Dunford and A. Capel, “A novel modeling method for photovoltaic cells.” *Power Electron. Specialists Conf.*, 2004.
- [37] Y. Yu, “Electric power system dynamics”, 1983.
- [38] D. Wenjuan, H. Wang and H. Cai, “Modelling a grid-connected SOFC power plant into power systems for small-signal stability analysis and control”, *Int. Trans. Electr. Energ. Syst.* vol. 23, pp. 330-341. 2013.

